Powder Technology 435 (2024) 119426

Contents lists available at ScienceDirect

Powder Technology

journal homepage: www.journals.elsevier.com/powder-technology

Estimation of mesoscale surface energy in the kinetic adhesion test

Lorenzo Pedrolli [a,b], Sadegh Nadimi [b,*], Beatriz Achiaga [a], Alejandro López [a,*]

[a] Department of Mechanics, Design and Industrial Management; University of Deusto, Bilbao, Spain
[b] School of Engineering, Newcastle University, Newcastle upon Tyne, United Kingdom

GRAPHICAL ABSTRACT

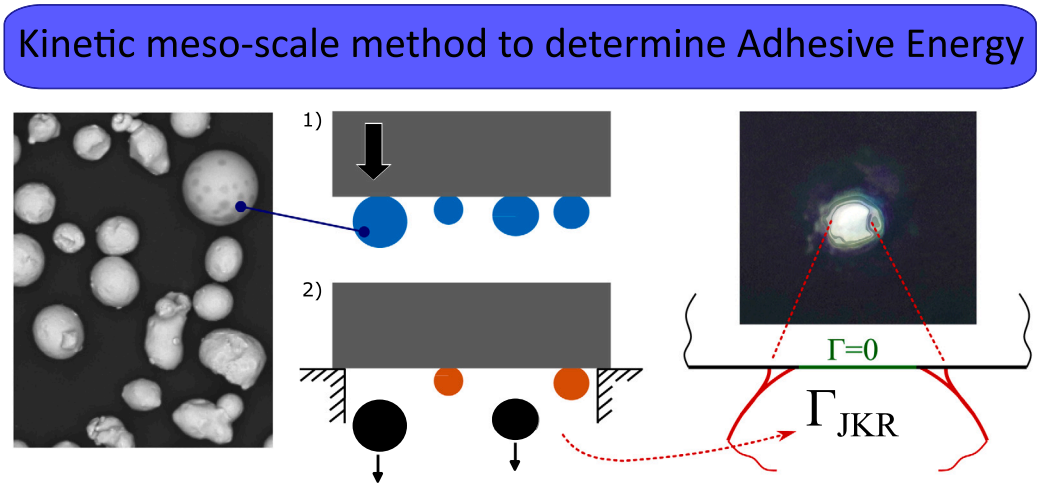

HIGHLIGHTS

- Derivation of the formula relating adhesive energy with kinetic energy during detachment.
- Description of the Kinetic Adhesion Test (KAT) procedure.
- Experimental validation of the proposed technique.
- DEM validation of KAT results using the JKR contact law.

ARTICLE INFO

MSC:
0000
1111

Keywords:
Interface energy
Adhesive energy
Adhesion measurement
Particle adhesion

ABSTRACT

The Johnson-Kendall-Roberts (JKR) contact model is widely accepted for the elastic adhesive contacts of particles. In this work, we present a novel interpretation of the JKR model that allows for the development of a test procedure with practical hardware called the Kinetic Adhesion Test.

The Kinetic Adhesion Test is based on the balance between kinetic and adhesive energy and allows for the determination of the mesoscale adhesive energy, Γ. The work not only presents the test procedure but also provides a derivation of the formula to determine Γ. This test procedure has been validated by experimental results compared with direct measurement of the contact radius.

* Corresponding authors.
E-mail addresses: Sadegh.Nadimi-Shahraki@newcastle.ac.uk (S. Nadimi), alejandro.lopez@deusto.es (A. López).

https://doi.org/10.1016/j.powtec.2024.119426
Received 8 September 2023; Received in revised form 9 January 2024; Accepted 12 January 2024
Available online 15 January 2024

Powder cohesion

Overall, the presented work provides a practical approach for determining adhesive energy, which is an essential factor in accurately simulating powder behaviour using DEM. This work contributes to the advancement of the accuracy of DEM simulations and, therefore, to the improvement of research in multiple fields, including materials science, engineering, and pharmaceuticals.

1. Introduction

Effective handling of fine powders is essential for numerous industrial processes, including food processing, mining, pharmaceuticals, and additive manufacturing. However, cohesive flows often present a significant obstacle, particularly when it comes to powder transport, leading to slow or even stalled operations. This is a common issue that must be addressed for many industries to function efficiently.

For certain processes, such as Laser Metal Deposition, it can be challenging to devise an alternative means of delivery, highlighting the importance of understanding the effects of particle adhesion. According to Singh et al. [1], comprehending and mitigating the impact of particle adhesion is critical for the advancement of this process. Therefore, exploring new ways to handle fine powders and improve transport is an ongoing priority for many industries.

Several commercial tools are available for the quasi-static bulk characterization of powder behaviour [2], providing information on the internal and wall angles of friction, flow initiation stress, bulk cohesion etc., by applying a compressing, shearing or tensile load to a powder bed. When translating the results of bulk characterization into DEM simulations, the contact model parameters must be determined through a calibration step. It is an empirical process, where the experiment is replicated digitally, and the mismatch between the real world and simulation is minimized through parameter exploration [3].

On the micro-scale, adhesion between fine particles and particle-surface is determined by a variety of interactions, such as Van der Waals (dispersion, dipole-induced-dipole, charge-fluctuation...) and Electrostatic (Coulomb, ionic, dipolar, hydrogen bonding...). Particle detachment and peeling experiments provide information on particle adhesion forces and the adhesion energies of solid surfaces in contact (i.e., attractive short-range forces) [4]. Such experiments are important in powder technology, xerography, ceramic processing, the making of adhesive films, and the understanding of granular flow and how cracks propagate in solids. Several methods, such as the pendulum, spring-balance (AFM), centrifugation, vibration, impact, and airflow, have been proposed to measure adhesion forces [5].

The proposed method falls in the impact methods category, which has the advantage of being a mesoscale type approach. It is able to capture the average behaviour of a small material sample, without recurring to AFM, and able to measure the interaction of a single particle, or bulk models. It lays its foundation in the widely accepted Johnson-Kendall-Roberts (JKR) contact model [6], which bases its formulation on the notion that a contact is essentially equivalent to a crack, and reads "the approach followed in this analysis, is similar to that used by Griffith in his criterion for the propagation of a brittle crack". For dissimilar surfaces, the Dupré work of adhesion is $\Gamma = \gamma_1 + \gamma_2 - \gamma_{12}$ [7], where γ_1 and γ_2 are the intrinsic surface energies of the solids, and γ_{12} the interface energy. The binding energy at the contact circle is defined as the surface energy per unit area of the surfaces multiplied by the contact circle area of radius a:

$$U_S = -\pi a^2 \Gamma \tag{1}$$

For similar surfaces, the Dupré work of adhesion can be simplified to $\Gamma = 2\gamma$, therefore Eq. (1) would become $U_s = -2\pi a^2 \gamma$. The contact radius a determined by the balance between surface (U_S), elastic (U_E) and potential energy from the applied load (U_P) is the base to derive the JKR contact model [6].

By accepting this definition, the implication relevant to this work is the connection of fracture mechanics to the adhesion of fine particles. The considerations that apply to fracture mechanics such as stiffening, bridging, and residual stress also apply to this field. The application of fracture mechanics to adhesive interfaces is explained by Kendall [8]. The proposed method in this work elaborates on the notion of the adhesive energy determination through an impact [9], treating the interface as a bond to be broken in an energy-driven event. This translates into a high strain rate, to which the adhesive energy is sensitive [8]. The centrifuge method used by many authors [10–12] can be seen as the quasi-static complement to the one proposed.

The energy description of the impact between elastic-adhesive particles is successful in the description of dust coagulation in space [13], a critical stage in planetary formation. The JKR contact model is one of the most adopted contact models in DEM simulations [14], for which adhesive energy is a critical parameter.

2. Theory/calculation

2.1. Energy balance

Johnson and Pollock [15] explore the original model [6] to find the response of colliding adhesive elastic particles. The surfaces' deformation is caused by the sphere inertia, $m\frac{d^2\delta}{dt^2}$, balanced by the total force at the interface P. In the case of a static contact, an external load P would cause a deformation δ.

In the article, displacement and forces are normalized as:

$$\overline{\delta} = \delta\left(\frac{\pi^2\Gamma^2 R}{3K^2}\right)^{-1/3} \quad \text{and} \quad \overline{P} = \frac{P}{3\pi\Gamma R} \tag{2}$$

Consequently, energies are normalized as:

$$\overline{U} = \left(\frac{9\pi^5\Gamma^5 R^4}{K^2}\right)^{1/3} \tag{3}$$

where:

$$\frac{1}{K} = \frac{3}{4}\left(\frac{1-\nu_1^2}{E_1} + \frac{1-\nu_2^2}{E_2}\right) = \frac{3}{4}\frac{1}{E^*} \tag{4}$$

At any given time, the total energy of the system U_T is the sum of the surface energy U_S, the stored elastic energy deriving from the surface deformation U_E and the mechanical energy introduced by the external load U_M. Johnson and Pollock [15] defined the internal energy in the system as the sum of elastic and surface energy:

$$U_I = U_E + U_S \tag{5}$$

and expressed the values in normalized form, denoted by the overline notation:

$$\overline{U_I} = \overline{U_E} + \overline{U_S} = \frac{\frac{6}{5}\overline{P_1}^2 + \overline{P_1} - \left(2\overline{P_1}\right)^{\frac{3}{2}}}{\overline{P_1}^{\frac{1}{3}}} \tag{6}$$

$$\overline{\delta} = \frac{3\overline{P_1} - \sqrt{8\overline{P_1}}}{\overline{P_1}^{\frac{1}{3}}} \tag{7}$$

The theory makes use of the normalized apparent Hertz load, where $P_1 = (K/R)\,a^3$ [6,15]. The effective external load is:

$$\overline{P} = \overline{P_1} - \sqrt{2\overline{P_1}} \tag{8}$$

By using this convention, Fig. 1 displays the contact model in terms of internal energy over displacement, with internal energy plotted on the Y-axis and displacement on the X-axis.

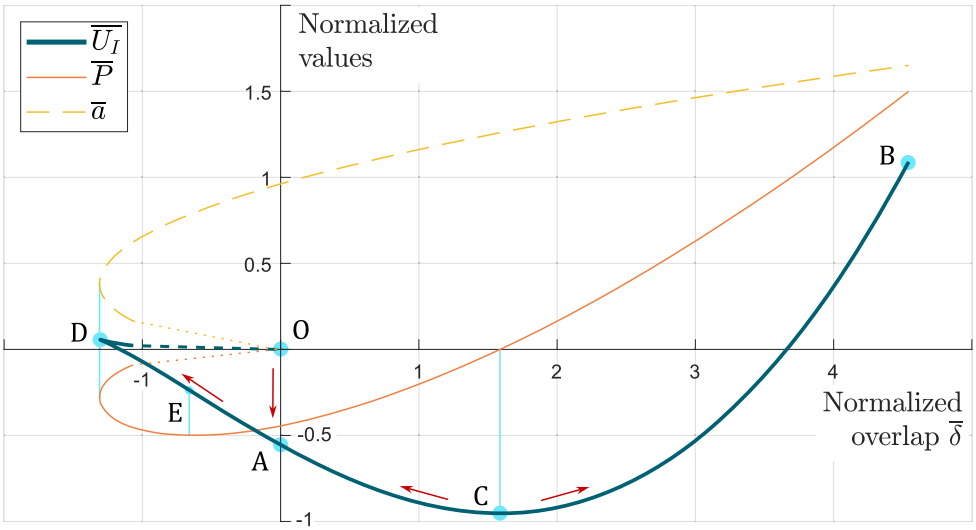

Fig. 1. Variation in normalized internal energy $\overline{U_I}$ as a function of normalized separation, as predicted by the J-K-R-S model of elastic sphere/flat contact with adhesion, by Johnson and Pollock [15]. The same graph also reports the normalized contact force ($\overline{P}$) and contact radius ($\overline{a}$) predicted by the contact model. The particle touches at O and snaps to A, initial non-equilibrium contact. Between D and O, no stable equilibrium is possible. C is the point of static equilibrium at zero load. E is the equilibrium at maximum negative imposed load; D static equilibrium at maximum imposed displacement. Energy is dissipated during snap-on O–A and snap-off D–O. Detaching from the equilibrium requires enough energy to cross C–D.

As the spherical particle approaches the surface, the energy remains zero until the contact point O for $\overline{\delta} = 0$, where the energy snaps to the value in point A. The energy $U_I(A) - U_I(O)$ is instantly dissipated in elastic waves. The static equilibrium of the contact is in point C, the minimum of U_I.

During an impact, the incoming particle with inbound kinetic energy T_i follows the curve through points $OACB$. If the energy is not enough, the particle oscillates around the equilibrium point C until the energy is dissipated through, therefore the energy state corresponds to the equilibrium.

During free fall, the interface is not subject to any additional external forces since the system is accelerating as a whole and is, therefore, essentially free from the influence of gravity. Before the impact with the stopping surface, the particles are in the energy well $U_I(C)$ and at the same time potential energy is being converted into kinetic energy T_{in}.

The critical condition can be determined by balancing the kinetic energy available to the particle with the total energy required for it to escape the energy well, from point C to point D of Fig. 1:

$$T_{crit} = U_I(D) - U_I(C) \tag{9}$$

The minimum value of Eq. (6) is $\overline{U_I}(C) = -0.95244$, obtained for $\overline{P_1} = 2$. Point D corresponds to the minimum overlap just before detachment. This is determined by calculating the minimum of Eq. (7) at $\overline{P_1} = \frac{1}{18}$, yielding $\overline{U_I}(D) = 0.05824$. Therefore, considering the normalization reported in Eq. (6):

$$T_{crit} = 1.0107 \left(\frac{9\pi^5 \Gamma^5 R^4}{K^2} \right)^{\frac{1}{3}} \tag{10}$$

The kinetic energy can be expressed as

$$T = \frac{1}{2} m v^2 = \frac{2}{3} \rho \pi R^3 v^2 \tag{11}$$

Solving Eqs. (10) and (11) for Γ gives:

$$\Gamma = v_i^{\frac{6}{5}} \cdot R_c \cdot \left(\frac{2^3 K^2 \rho^3}{3^5 \pi^2 (1.0107)^3} \right)^{\frac{1}{5}} \tag{12}$$

where R_c is the critical radius, or the size of the biggest particle able to stay attached to the surface, and v_i is the velocity at the moment of impact. The same formula can be used if considering the potential gravitational energy since, for the simple case of a falling object from a standstill, the impact velocity would be directly related to the dropping height h by $v = \sqrt{2\,gh}$.

As mentioned in the Introduction, the JKR solution for the adhesion of elastic spheres [6] is conceptually identical to Griffith's theory of elastic fracture [16]. By balancing the load's potential energy, strain energy, and the surface energy of the crack faces, Griffith derived the criterion for stability of a crack of length $2c$ in an infinite elastic sheet, with tensile stress σ applied in the orthogonal direction of the slit. As a sanity check, the reader can recall the theory to express the fracture criterion in terms of adhesive energy, to compare the magnitude of the values obtained. The proposed mesoscale approach is well suited to be compared with Linear Elastic Fracture Mechanics, as it shares many of the underlying assumptions. Conversely, the adhesive energy values obtained with this method might not be compared on the micro-scale, where different assumptions are necessary.

3. Test procedure

The Kinetic Adhesion Test (KAT) is divided into five phases, represented in the flow diagram of Fig. 2.

3.1. Particle distribution

Proper particle sampling and dispersion onto a substrate are critical steps for accurately representing the Particle Size Distribution (PSD) of powders. Manual or dedicated distribution tools can be used to ensure optimal dispersion and avoid overcrowding, which facilitates subsequent processing stages. The dispersion of powders is complex and requires guidance from relevant literature, such as [17]. Determining the correct width of the PSD is crucial, as it affects the amount of data that needs processing. Once particles are dispersed without clustering, the following steps use relative assessments to determine cohesion, and sample segregation should have a limited influence on the results.

The substrate must be prepared according to the measurement requirements. In the present work, the smooth surfaces were cleaned using a 50%–50% solution of acetone in water, and dried in ambient air. Surface roughness, contamination and humidity can be introduced to represent the desired real-case scenario, determining the mesoscale adhesive energy.

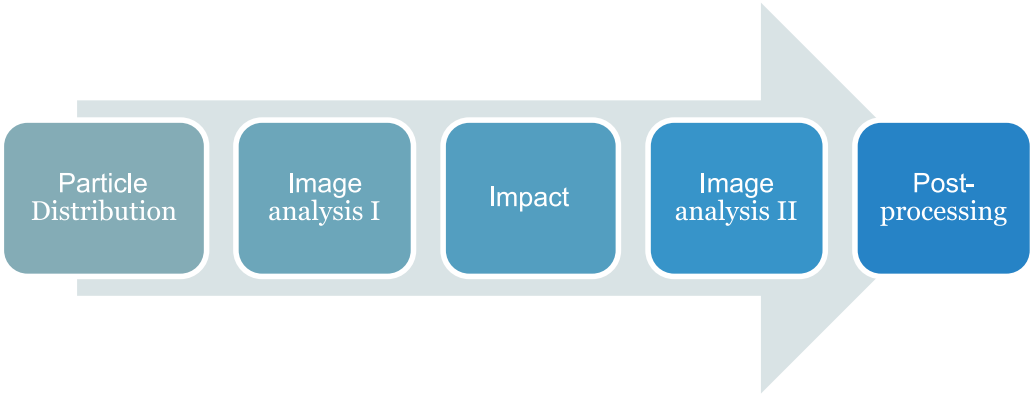

Fig. 2. Flow diagram of the Kinetic Adhesion Test.

3.2. Image analysis I

In this work, the powder sample was analysed by means of an optical microscope. The images were digitized for a resulting resolution of 1.05 μm/px. The objective is to obtain at least 10 px per particle diameter, which is the minimum required for viable diameter information [18]. Using the open-source Fiji image processing tool [19], the microscopic images were filtered, labelled and the resulting binary image was used to determine the PSD: one of the acquired images is presented in Fig. 5(a). Fig. 6 reports an expected distribution. This semi-automatic process allowed for the consideration of samples composed of up to several thousand particles.

3.3. Impact

The suggested testing approach employs the hardware described technically in [20] and shown in Fig. 3. The open-source design files are stored in an open-access repository [21]. It allows recording the velocity of the falling sample at the moment of impact with the surface. The hard impact grants an almost instantaneous stop of the substrate, while the particles' momentum must be balanced by the adhesive energy, as described in Section 2.1. In this phase, the larger particles tend to detach while smaller ones do not, as is represented in Fig. 4.

3.4. Image analysis II

The PSD is determined again for the sample after the impact, with a procedure similar to 3.2. An example image is Fig. 5(b). In an ideal case, the resulting distribution is truncated at a specific diameter d_C, and the cumulative curve consequently changes (see Fig. 6).

3.5. Post-processing

The two PSDs before and after the test are then compared. If no unexpected deviation occurs, the distribution is truncated at the critical diameter d_C. In an ideal case of perfectly spherical particles and uniform adhesion, Fig. 6 displays how the PSD changes before and after the test, indicating the critical diameter. Smaller particles constitute a bigger fraction of the total after the impact, therefore the PSD curve after the impact should be steeper and end sharply at the top. After acquiring the exact drop velocity and the exact critical diameter, Eq. (12) is used to determine the adhesive energy Γ.

The deviation from the ideal case results in a distorted PSD after the test. Therefore, the proposed test is able to quantify the mesoscale adhesive energy between particles and a substrate. It is expected that each individual particle presents a slightly different adhesive bond. Reasons include and are not limited to particle shape, particle and/or substrate roughness, uneven interface oxidation or contamination. Also, if only a small number of larger particles compose the sample, the distribution (closer to unity) might get distorted.

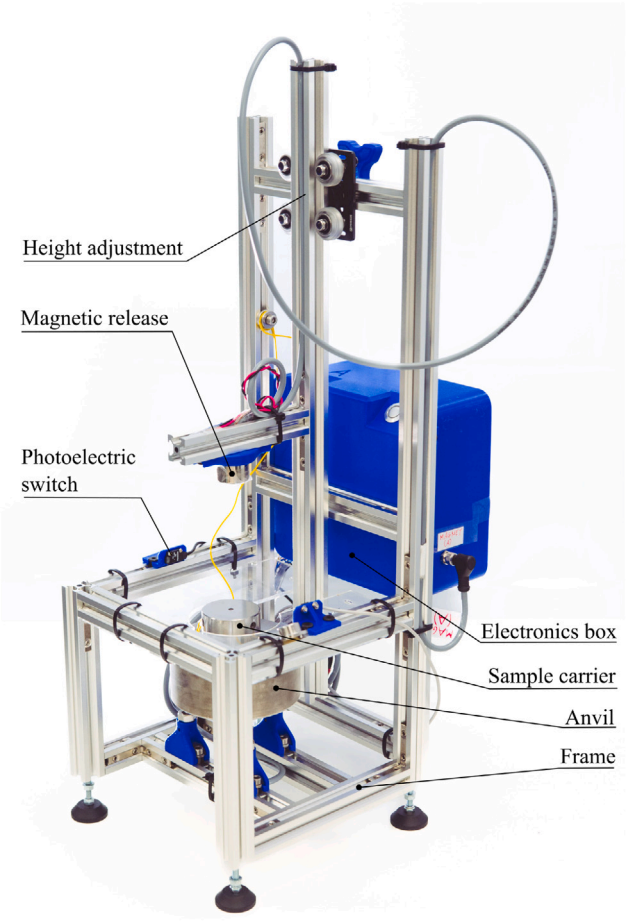

Fig. 3. Annotated view of the test device [20].

In Shimada et al. [10], a centrifuge method measured particle adhesive strength on a substrate, defining critical diameter as the average size range for 50% particle removal. A similar metric applies to the proposed method. Results showed medium-sized particles had the highest adhesion strength, while smaller and larger particles had lower strength. This effect can also deviate the PSD after the proposed test from the ideal case.

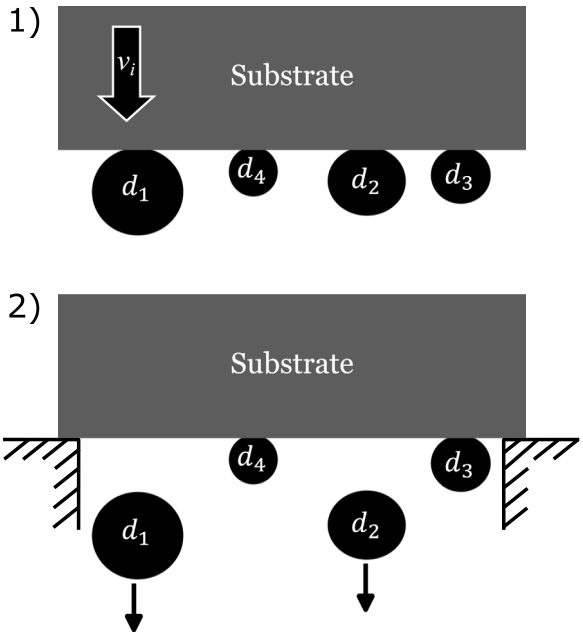

Fig. 4. Sketch depicting the detachment of the particles during the impact, from (1) to (2).

Table 1
Material properties used in this study.

	ρ [kg m^{-3}]	E [Pa]	ν [−]
316L Stainless steel [23]	7980	2.11e11	0.3
Borosilicate glass (TedPellainc.)	2510	7.3e10	0.2
UPVC film (azom.com)	1440	3.0e9	0.3

4. Results

Initial validation has been carried out using a stainless steel metal powder on a polymer film and on a microscope glass slide, for which the material characteristics are presented in Table 1.

Easterling and Thölén [22] used the same JKR contact model, measuring the geometry of the contact (a_0) to determine the adhesion between metallic particles observed through electron microscopy: the interface energy for Fe-Ni contact was estimated to be in the order of 6 J/m^2. In this section, the contact radius a_0 is measured using optical microscopy.

4.1. Polymeric film

The polymeric film has been securely adhered to a stiff substrate in the carrier. A small sample of metallic powder was carefully distributed on the substrate, from a low drop height. The dispersion was carried out manually, given the forgiving nature of the powder under analysis, but an automatic tool would have greatly helped in guaranteeing a better, uniform dispersion [17].

The test was conducted at room temperature and humidity (approx. 20 °C, RH 50%); no particular tool was used to eliminate static charges. PSD was determined through optical microscopy and image analysis, as reported in Fig. 7. The sample was loaded in the apparatus, and it impacted the anvil at a velocity of $v_i = 1.40$ m/s. The same optical method has been used to determine the PSD after the impact, also reported on the same graph. The imaged sample is composed of about 500 particles before the impact and 340 after. The image resolution for this case is 0.93 μm/px.

The PSD is reported in Fig. 7, from which it is possible to determine the critical size or the diameter of the largest particle still attached to the substrate after the impact. The PSD changed as expected, with a little deviation from the ideal case of Fig. 6. This can be attributed to the non-perfect sphericity and smoothness of the particles and the fact that only a few elements represent the higher side of the distribution. The critical diameter determined from the PSD in Fig. 7 is $d_C = 46$ μm.

Using the values of this case from Table 1 and Eq. (4) we obtain $K = 4.33e9$ Pa. Eq. (12) is then used to determine the interface's Adhesive Energy, resulting in $\Gamma_{KAT} = 17.53$ J/m^2.

The same polymeric film has been carefully extended in support spanning a distance of 15 mm, applying a negligible stretch to avoid sagging. A small sample of particles was distributed on the surface, and the sample was flipped upside-down. By employing a reflective optical microscope it was possible to image the contact point of the particles and, by switching the focus, the diameter of the same particle. An example is reported in Fig. 9. Since the contact could be irregular, the equivalent contact diameter is assumed to be $a_0 = \sqrt{A/\pi}$.

At equilibrium, the contact radius of the spherical particle on a surface is a_0 [6]:

$$a_0^3 = \frac{6\Gamma\pi R^2}{K} \tag{13}$$

which can be rewritten to express the surface energy Γ:

$$\Gamma = a_0^3 \frac{K}{6\pi R^2} \tag{14}$$

Using this formulation, the example reported in Fig. 9 has a value $\Gamma_{a0,1} = 18.1$ J/m^2. A sample of 8 particles gave as a result an average of $\Gamma_{a0} = 19.8$ J/m^2, with standard deviation $\sigma_{a0} = 4.4$ J/m^2.

The contact area has been observed optically to be delimited by the first Newton ring; this is acceptable given the expected contact geometry. Johnson et al. [6] analytically derived the deformed shape of the contact. The stress at the contact's edge tends to form a neck, Fig. 8 represents it visually. For this reason, it is assumed that the first visible edge is indeed the contact's edge. This technique, analysed by Raedler and Sackmann [24] and by Waschke et al. [25], in its more complete form is called Reflection Interference Contrast Microscopy (RICM), and is an appropriate method to determine the contact radius of particles on a flat, transparent substrate.

4.2. Borosilicate glass

The same procedures were followed changing the substrate material to borosilicate glass, whose characteristics are reported in Table 1. In this case, the test has been conducted two consecutive times with increasing impact speeds. Fig. 10 reports the PSD of the test. It is interesting to note that the shape of the distribution is somewhat preserved between the three curves, as expected from the considerations in 3.5.

Case A: impact speed $v_i(A) = 2.21$ m/s. The critical diameter $d_C(A) = 52.9$ μm determines an adhesive energy of $\Gamma_{KAT}(A) = 103.34$ J/m^2.

Case B: $v_i(B) = 2.96$ m/s; $d_C(B) = 35.6$ μm; $\Gamma_{KAT}(B) = 98.78$ J/m^2.

The images in Fig. 5 are relative to Case A, for which the expected values are in line with the ones determined in this section.

The use of a thin slide allowed us to see through the glass, and capture an image of the contact surface as with the previous case. The measured value across 8 samples is $\Gamma_{a0} = 95.4$ J/m^2. A wide standard deviation of 34 J/m^2 was observed. Adhesion phenomena exhibit inherent stochastic characteristics, particularly within the mesoscale considered in this study. The substantial dispersion observed suggests that particles, adhering to the surface in random orientations, possibly interact with the surface with a degree of variability. One hypothesis is that, for these higher Adhesive Energy values, some particles can stick in unfavourable orientations, while others either fall or reorient to touch the surface in more favourable spots.

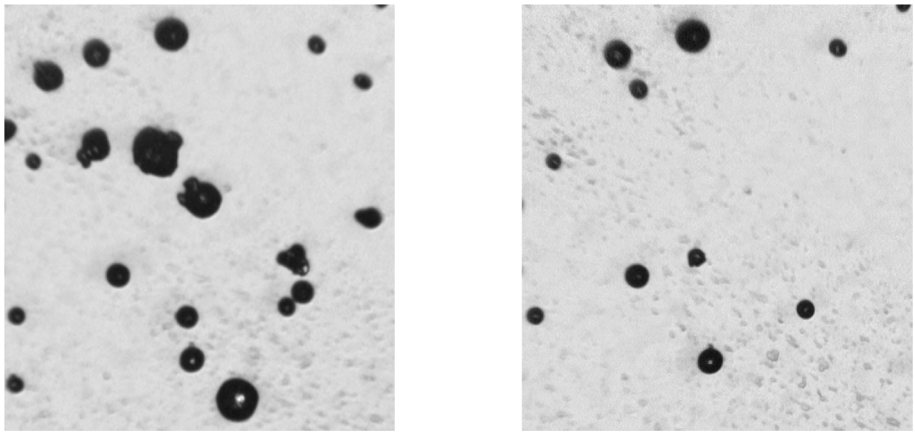

(a) Sample before the test. (b) Sample after the test.

Fig. 5. Example of the microscopy images captured before and after the impact ($v_i = 2.21$ m/s), carefully picked to show the same location. 316L steel powder sample on a glass substrate. The maximum diameter after the impact (particle at the top) is 39 μm, which is compatible with the values determined in Section 4.2.

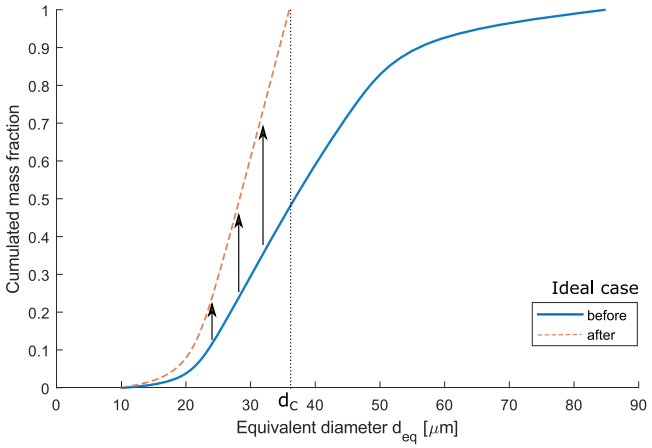

Fig. 6. Ideal case of a cumulative PSD before and after the test.

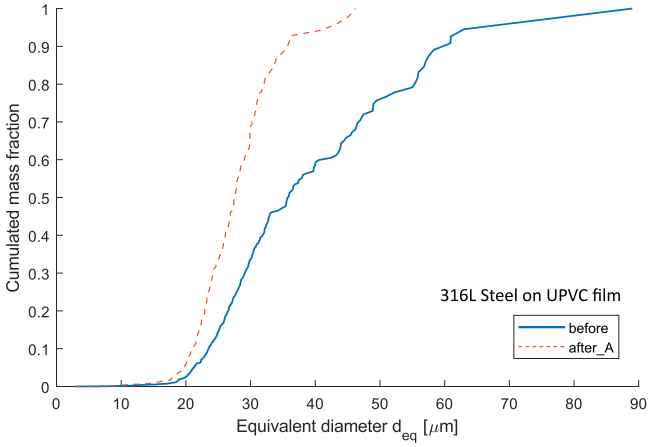

Fig. 7. Cumulative mass distribution of 316L stainless steel powder particles on a UPVC film, measured before and after the impact. The calculated adhesive energy in this case is $\Gamma_{KAT} = 17.53$ J/m^2..

4.3. Strain-rate dependency

The influence of strain rate on adhesive energy is explored through analytical and molecular dynamics approaches in two distinct papers.

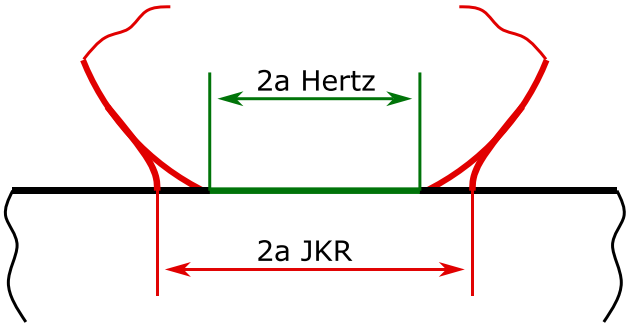

Fig. 8. Contact shape comparison between the purely-elastic Hertz and adhesive-elastic JKR models.

The analytical study by Kendall [8] delves into strain-rate dependency during detachment, revealing a tendency for the apparent adhesive energy to increase. The work provides valuable insights into the formation and fracture of adhesive interfaces between rubber and glass, with a particular focus on the influence of strain rate. The experiments involved applying forces to propagate interfacial cracks, revealing complex kinetics and hysteresis phenomena akin to liquid droplets wetting solid surfaces. Notably, Kendall observed an increase in adhesion with contact time and crack speed, introducing the concept of Adhesive Energy (Γ), encompassing both reversible and irreversible work. The molecular dynamics investigation conducted by Chowdhury and Gillespie [26] utilizes simulations to elucidate the strain-rate-dependent behaviour of adhesive contacts mediated by silane groups on glass surfaces.

The work from Zafar et al. [9] reports values obtained from a setup compatible with the one used for this work. In their drop test, they measured the falling velocity of the stub, onto which a silanized glass was dispersed on a silanized glass substrate. The paper reports the values for *Impact Velocity* and *Critical Diameter* resumed in Table 2. The material properties used for the borosilicate glass are in Table 1.

With only these two values and the material properties it is possible to apply Eq. (12), obtaining the *Adhesive Energy* Γ.

A further verification step can be performed. Adhesive energy can be determined by considering the deceleration the particles are subjected to. Thornton [14] reports a formula to determine the critical impact time or the duration of a Hertzian elastic impact of a spherical particle on a flat surface [27]:

$$t_c = 2.865 \left(\frac{m^2}{RE^{*2} v_i} \right)^{1/5} \tag{15}$$

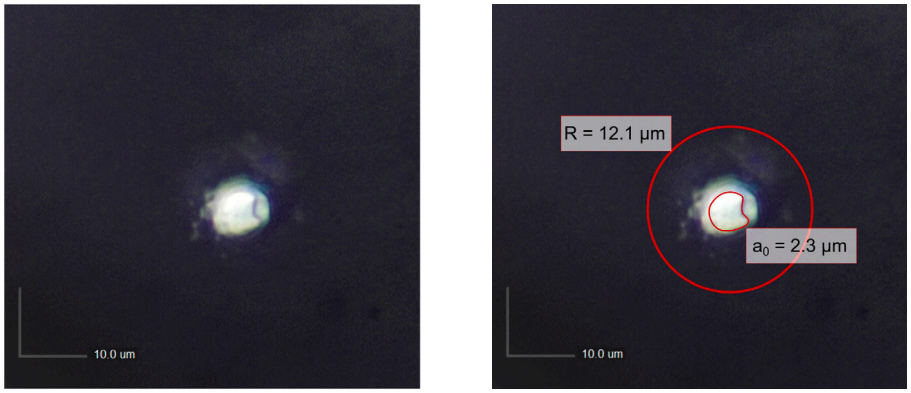

Fig. 9. Optical microscope image of the contact of one 316L stainless steel powder particle on UPVC film.

Table 2
Impact velocity and critical diameter determined by Zafar et al. [9]. Adhesive energy Γ is determined using the method proposed in this work. Calculations were repeated by using the theoretical time needed for a normal rebound [14] and the corresponding deceleration.

Impact velocity v_i [m/s]	1.8	2.3	3.0	4.1	4.8	5.4	6.0
Critical Diameter d_c [µm]	66.4	63.8	59.8	53.0	47.5	42.3	37.3
Adhesive Energy Γ [J/m^2]	44.8	57.7	74.5	96.0	103.9	106.6	106.7
Rebound time [14] t_r [ps]	201.3	184.2	163.7	136.3	118.4	103.0	88.9
Detachment time $t_d \approx t_r/2$ [ps]	100.7	92.1	81.9	68.2	59.2	51.5	44.4
Gamma considering detachment time Γ_{td} [J/m^2]	44.0	56.7	73.1	94.3	102.1	104.7	104.8

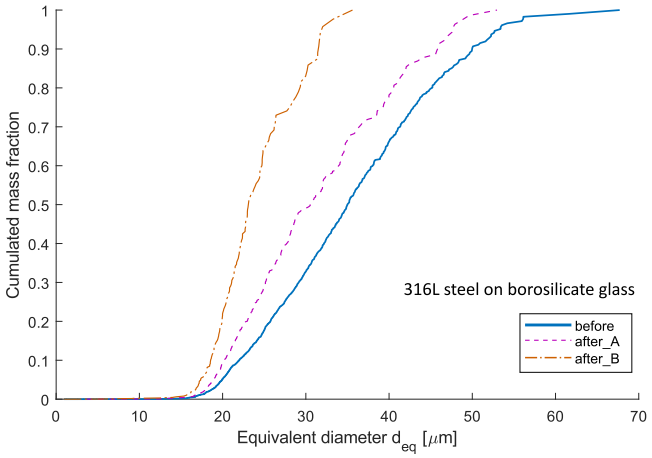

Fig. 10. Cumulative mass distribution of 316L stainless steel powder particles on a borosilicate glass slide, measured before and after the impacts.

As a crude approximation, we can consider the detachment time t_d to be half of that. Both values are reported in Table 2, but it must be clear that this formula is exact for the mentioned conditions, and the adhesive term can generate significant discrepancies. The adhesive energy can be estimated by equating the detachment force to the adhesive force, as proposed by Zafar et al. [9]. However, in this case, the detachment force values would be determined by $F_{det} = mv_i/t_d$.

$$\frac{F_{det}}{F_{ad}} = \left(\frac{mv_i}{t_d}\right) / \frac{3}{2}\pi R_c \Gamma_{td} = 1 \tag{16}$$

therefore

$$\Gamma_{td} = \frac{8}{9}\rho R_c^2 \frac{v_i}{t_d} \tag{17}$$

resulting in the values reported in Table 2, which are consistently 1.8% lower than the ones determined by Eq. (12). This difference is compatible with the approximation of the detachment time, which is considered a perfectly elastic impact.

Given these considerations, we can trace the graph of Fig. 11, which shows a dependency of the adhesive energy to the impact velocity, which is related to the strain rate of the contact given its influence on t_c. Faster impacts determine a faster strain rate of the contact. Silane groups on the glass surface greatly increase their cohesion. Chowdhury and Gillespie [26] performed molecular simulation precisely to determine whether the strain rate has an influence on glass adhesive contacts mediated by silane groups. Different domains are highlighted in the research, based on both the bond strength (in [GPa]) and the adhesive energy (in [J/m^2]). Domain 1 corresponds to low strain rates and the lowest values for both the bond strength and adhesive energy, where a weak dependency is highlighted. Domain 2 is a transition towards the much higher values of Domain 3. Their argument is that the specific chemical interlacing mediated by the silane groups on the surfaces change their response to a high strain rate detachment. When the bond breaks gradually, molecular thermal movements assist in separating it. However, as the strain rate increases, there is less time for these molecular movements to untangle the bond, leading to a gradual increase in adhesive energies. This trend continues until it reaches a maximum, where the molecular groups separate abruptly, primarily without relying on thermal movements. The maximum values reported by the paper are between 80 J/m^2 and 120 J/m^2, depending on the surface concentration of silane groups. The adhesive energy values obtained by this work, reported in Fig. 11, appear to correspond to Domains 2 and 3, where the transition tapers off on the higher end of strain rates.

5. DEM model

The particle response normal to the surface is the most relevant to the presented Kinetic Adhesion Test, and a simplified representation is provided in Fig. 12. Most DEM codes have an implementation of the purely elastic Hertz-Mindlin contact model: once the particle enters contact with the surface, the reaction force can be modelled by a non-linear spring whose elastic constant is related to the material properties and the particle size [28]. The tangential force model is based on the Mindlin–Deresiewicz work [29,30], but is not relevant for the simulation of this test. Additionally, a damping force F_d is applied where the damping coefficient is related to the coefficient of restitution according to the work by Tsuji et al. [31]. This translates to a certain measure of viscous dissipation, which has the collateral effect of contributing to numerical stability.

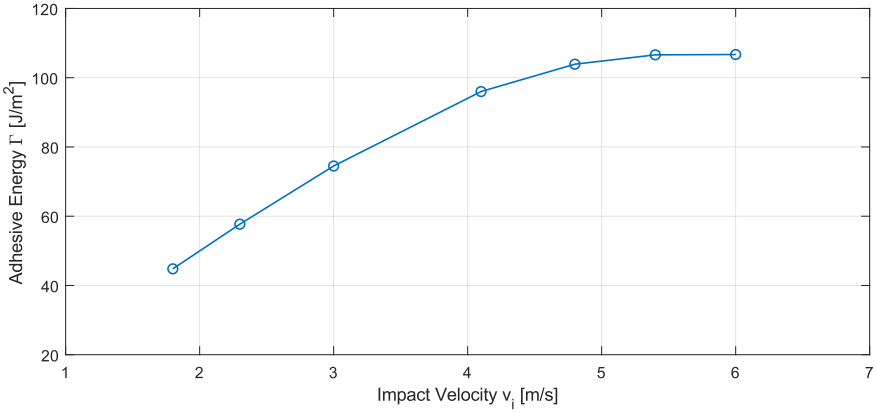

Fig. 11. Adhesive Energy values of silanized glass beads on silanizad glass substrate [9]. The values are those of Table 2.

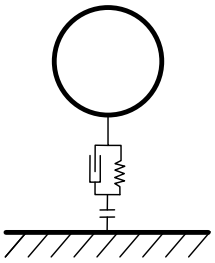

Fig. 12. Simplified representation of the Spring-Slider-Dashpot (SSD) system representing the contact normal to a surface of a spherical particle.

The JKR contact model, previously discussed and represented in Fig. 1, is implemented in EDEM as "*Hertz-Mindlin with JKR Version 2*" where the normal force is adhesive-elastic according to Johnson et al. [6], and the damping force is the same as the pure Hertz-Mindlin model.

To have a simulation representing the test, a surface is placed in the origin, and a large number of particles are dispersed onto it. The spherical particles interact exclusively with the surface, not with each other. The first phase of the simulation is run until the particles settle to a null velocity. The particles' size is determined by a random distribution to cover a useful size range around the expected critical diameter, roughly matching the size range of the experiment.

The following result is used to validate the case of 316L stainless steel particles on UPVC film. A similar analysis was conducted for the data on glass substrate, with similar results. In the simulation, particle size is a uniform distribution from 30 μm to 72 μm. Material properties correspond to the 316L stainless steel and UPVC film already reported in Table 1, and the spherical particles are allowed to interact exclusively with the substrate plane. The normal model is set to JKR, with a surface energy of 17.53 J/m^2, the same value as the measurement reported in Section 4.1.

The substrate is accelerated to the desired falling velocity, the particles are pressed into the surface and accelerate with it. Once the velocity is reached, it is maintained constant until the particles have stabilized. The coefficient of restitution is set to a very high value $e = 0.99 - 0.999$, to interfere as little as possible with the detachment. It is used to provide some numerical damping during the rest of the simulation, by setting it to a lower value. If the restitution coefficient is set to unity, the particles would oscillate indefinitely around the equilibrium position and velocity. Gravity is considered in the simulation both on the particles and the substrate.

Once the simulation is stable, with the substrate and particles falling at the same velocity, the substrate velocity is immediately set to zero, effectively realizing a step input. From the simulation, we expect the particles to detach if their diameter is larger than a critical diameter, with a velocity that corresponds to the residual kinetic energy after breaking the contact. Fig. 13 represents the result of the simulation after the substrate stops at $t = 0.0002$. Some additional time is allowed to pass to allow the kinetic energy of the smaller particles to be dissipated in oscillations around the equilibrium.

We recall as expected value the obtained critical diameter from Fig. 7. Indeed, running the simulation leads to particles detaching for a critical diameter of $d_c = 46.0$ μm, as highlighted from the graph in Fig. 14. Smaller particles dissipate all their kinetic energy by oscillating around the equilibrium through viscous dissipation. Larger particles detach from the surface, retaining an increasing fraction of their kinetic energy acquired during the drop, determining a velocity that tends asymptotically to the value just before the impact for larger and larger particles. A similar result can be obtained for the stainless steel powder dispersed on borosilicate glass.

As mentioned, the presented test is able to give a representative value for the adhesive energy Γ of the interface between particle and substrate. This mesoscale values does not differentiate between the contribution of some real-world features such as surface roughness, contact plasticization, liquid bridges, and electrostatic charge. This work follows the considerations of the JKR contact theory [6], ensuring an agreement between the underlying assumptions. For this reason the calculated Adhesive Energy values are useful in simulation, resulting in a good agreement of the considered quantities whenever the same JKR contact model is used.

6. Conclusion

When dealing with particulate matter, it is critical to represent the impact between particles or the particle–wall interaction using an appropriate contact model. The JKR contact model [6] adapts Griffith's theory to the contact between an adhesive elastic sphere with a flat surface. To this day, it is a widely accepted adhesive-elastic model and is frequently employed in DEM simulations. One of the critical parameters is the adhesive energy Γ, which is closely related to the energy release rate defined in Linear Elastic Fracture Mechanics [8]. Breaking a contact is essentially similar to crack growth. This work presents a novel interpretation of the JKR contact model [6] expressed in energy terms [15], in order to determine the adhesive energy of materials. The derived formula presented in this work determines the test strategy. The test is intended to define the mesoscale behaviour of the powder, rather than the micro-scale. Therefore, the proposed technique differs substantially from the classification of the adhesion-measurement techniques reported by Israelachvili [4], among which the impact method is mentioned.

This approach differs in its fundamental assumptions from similar methods: the existing works on impact-based methods assume that

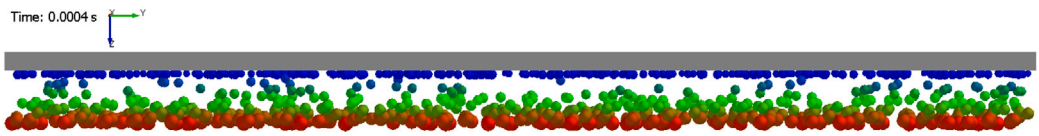

Fig. 13. Result of the simulation — 316L steel powder on UPVC film. The particles are coloured according to the velocity, and the substrate is represented in grey. Bigger particles were able to detach and proportionally retained more kinetic energy. Smaller particles did not detach and their kinetic energy was dissipated in the oscillations around equilibrium.

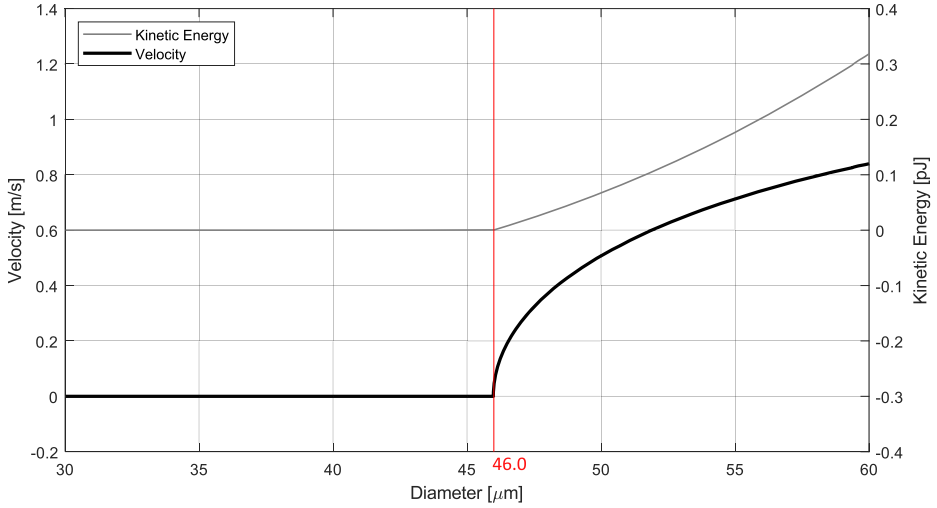

Fig. 14. Result of the simulation — 316L steel powder on UPVC film. The critical diameter obtained from the simulation is highlighted by the vertical line. Bigger particles were able to detach and proportionally retained more kinetic energy, for a residual velocity asymptotically approaching the velocity before the impact. Smaller particles did not detach and their kinetic energy was dissipated in the oscillations around equilibrium.

particles are detaching when they hit a maximum value of the force F_{po} [9], in a similar way as centrifuge methods [11], which implies that detachment essentially happens under the action of a constant force. This is certainly true for centrifuge methods, where the same apparent centrifugal acceleration can be maintained indefinitely. In this work we assume that the particles detach using the energy available just before the impact, their kinetic energy. This results in an analytical interpretation of the work by Johnson and Pollock [15], used to evaluate the adhesion in some test cases.

The proposed method is aimed at DEM simulations, where the adhesive energy value allows to model the behaviour of cohesive material using the JKR contact model. This mesoscale approach results in a relatively easy and quick procedure to obtain such values, to be used in simulations where the microscopic features and interactions are not modelled.

The fundamental assumption of the energy balance between adhesion and kinetic energy could be adapted to use different assumptions on the material behaviour (DMT, M-D, damping forces), matching the choice made when setting up the DEM simulation. An elasto-plastic adhesive contact model can be used on the basis of this work, such as the one proposed by Pasha et al. [32]. However, such models generally require more knowledge of the contact history and material properties (yield behaviour). As mentioned, the presented formulation does not differentiate between the adhesion mechanisms (Van der Waals, liquid bridge, plasticization, ...), resulting in a mesoscale description of the adhesive energy. A DEM simulation of the test confirms the validity of the proposed approach and the compatibility between the analytical and numerical models.

The adhesive energy values of Γ determined with the presented Kinetic Adhesion Test have been experimentally verified through the direct measurement of the contact radius a_0 on a selection of materials. Also, the predictive ability of the model is confirmed using DEM simulation. Adhesive Energy values obtained in this work are used to simulate the test itself, correctly matching the critical diameter observed in the experiments.

Values obtained from literature for silanized glass surfaces [9] are compared with Molecular Dynamics simulations by Chowdhury and Gillespie [26]. The proposed interpretation allows to close the gap between the two works, obtaining comparable Adhesive Energy values. These increase up to a plateau with increasing impact velocities, matching the strain rate evidenced by the Molecular Dynamics study, suggesting a correlation. This work only confirms the plausibility of the calculated Adhesive Energy. The correlation between impact velocity and strain rate is not explored here, whereas a dependency of the Adhesive Energy on the strain rate is explained by Kendall [8].

Future work could involve determining the statistical adhesion variability through the PSD [10], therefore resulting not in a single adhesive parameter, but in an average and a standard deviation representative of the entire sample. This variability is expected especially with contamination and rough particles, which are present in any realistic scenario.

Ethics statements

This work does not have any outstanding ethical implications.

CRediT authorship contribution statement

Lorenzo Pedrolli: Data curation, Formal analysis, Investigation, Methodology, Validation, Writing – original draft, Writing – review & editing, Conceptualization. **Sadegh Nadimi:** Conceptualization, Funding acquisition, Investigation, Project administration, Resources, Supervision, Writing – review & editing. **Beatriz Achiaga:** Formal analysis, Supervision, Writing – review & editing, Conceptualization. **Alejandro López:** Conceptualization, Funding acquisition, Project administration, Supervision, Writing – review & editing.

Declaration of competing interest

The authors declare that they have no known competing financial interests or personal relationships that could have appeared to influence the work reported in this paper.

Data availability

Data will be made available on request.

Acknowledgements

This project has received funding from the European Union's Horizon 2020 research and innovation programme under the Marie Skłodowska-Curie grant agreement No. 847624. In addition, a number of institutions back and co-finance this project. The content of this work reflects only the author's view, the Agency is not responsible for any use that may be made of the information it contains.

The authors would like to acknowledge the contribution of the Engineering and Physical Sciences Research Council, EPSRC reference EP/V053655/1, for designing and building the KAT setup employed in this study.

References

[1] A. Singh, S. Kapil, M. Das, A comprehensive review of the methods and mechanisms for powder feedstock handling in directed energy deposition, Addit. Manuf. 35 (2020) 101388, http://dx.doi.org/10.1016/j.addma.2020.101388, URL: https://www.sciencedirect.com/science/article/pii/S2214860420307600.

[2] M. Ghadiri, M. Pasha, W. Nan, C. Hare, V. Vivacqua, U. Zafar, S. Nezamabadi, A. Lopez, M. Pasha, S. Nadimi, Cohesive powder flow: Trends and challenges in characterisation and analysis, KONA Powder Part. J. 37 (2020) 3–18, http://dx.doi.org/10.14356/kona.2020018.

[3] M. Alizadeh, M. Asachi, M. Ghadiri, A. Bayly, A. Hassanpour, A methodology for calibration of DEM input parameters in simulation of segregation of powder mixtures, a special focus on adhesion, Powder Technol. 339 (2018) 789–800, http://dx.doi.org/10.1016/j.powtec.2018.08.028, URL: https://www.sciencedirect.com/science/article/pii/S0032591018306442.

[4] J.N. Israelachvili, Intermolecular and Surface Forces, Academic Press, 2011.

[5] K. Higashitani, H. Makino, S. Matsusaka, Powder Technology Handbook, CRC Press, Taylor & Francis Group, 2020.

[6] K. Johnson, K.K. A., D. Roberts, Surface energy and the contact of elastic solids, Proc. R. Soc. Lond. Ser. A Math. Phys. Eng. Sci. 324 (1558) (1971) 301–313, http://dx.doi.org/10.1098/rspa.1971.0141.

[7] S. Ebnesajjad, 3 - Surface tension and its measurement, in: S. Ebnesajjad (Ed.), Handbook of Adhesives and Surface Preparation, in: Plastics Design Library, William Andrew Publishing, Oxford, 2011, pp. 21–30, http://dx.doi.org/10.1016/B978-1-4377-4461-3.10003-3, URL: https://www.sciencedirect.com/science/article/pii/B9781437744613100033.

[8] K. Kendall, Cracks at adhesive interfaces, J. Adhes. Sci. Technol. 8 (11) (1994) 1271–1284, http://dx.doi.org/10.1163/156856194x00609.

[9] U. Zafar, C. Hare, A. Hassanpour, M. Ghadiri, Drop test: A new method to measure the particle adhesion force, Powder Technol. 264 (2014) 236–241, http://dx.doi.org/10.1016/j.powtec.2014.04.022.

[10] Y. Shimada, M. Tsubota, S. Matsusaka, Measurement of particle adhesion force and effective contact radius via centrifuge equipped with horizontal and vertical substrates, Powder Technol. 397 (2022) 117103, http://dx.doi.org/10.1016/j.powtec.2021.117103, URL: https://www.sciencedirect.com/science/article/pii/S0032591021011219.

[11] S. Kinugasa, S. Tanoue, Y. Shimada, S. Matsusaka, Detailed analysis of particle–substrate interaction based on a centrifugal method, Adv. Powder Technol. 33 (11) (2022) 103793, http://dx.doi.org/10.1016/j.apt.2022.103793, URL: https://www.sciencedirect.com/science/article/pii/S0921883122003727.

[12] P.G.C. Petean, M.L. Aguiar, Determining the adhesion force between particles and rough surfaces, Powder Technol. 274 (2015) 67–76, http://dx.doi.org/10.1016/j.powtec.2014.12.047, URL: https://www.sciencedirect.com/science/article/pii/S0032591014010298.

[13] A. Chokshi, A.G.G.M. Tielens, D. Hollenbach, Dust coagulation, Astrophys. J. 407 (1993) 806, http://dx.doi.org/10.1086/172562.

[14] C. Thornton, Granular Dynamics, Contact Mechanics and Particle System Simulations : a DEM Study, Springer-Verlag GmbH, 2015, p. 195.

[15] K. Johnson, H. Pollock, The role of adhesion in the impact of elastic spheres, J. Adhes. Sci. Technol. 8 (11) (1994) 1323–1332, http://dx.doi.org/10.1163/156856194x00636.

[16] A.A. Griffith, G.I. Taylor, VI. The phenomena of rupture and flow in solids, Phil. Trans. R. Soc. Lond. Ser. A 221 (582–593) (1921) 163–198, http://dx.doi.org/10.1098/rsta.1921.0006, URL: https://royalsocietypublishing.org/doi/10.1098/rsta.1921.0006.

[17] G. Calvert, M. Ghadiri, R. Tweedie, Aerodynamic dispersion of cohesive powders: A review of understanding and technology, Adv. Powder Technol. 20 (1) (2009) 4–16, http://dx.doi.org/10.1016/j.apt.2008.09.001.

[18] V. Angelidakis, S. Nadimi, M. Garum, A. Hassanpour, Nano-scale characterisation of particulate iron pyrite morphology in shale, Part. Part. Syst. Charact. n/a (2022) 2200120, http://dx.doi.org/10.1002/ppsc.202200120, URL: https://onlinelibrary.wiley.com/doi/abs/10.1002/ppsc.202200120.

[19] J. Schindelin, I. Arganda-Carreras, E. Frise, V. Kaynig, M. Longair, T. Pietzsch, S. Preibisch, C. Rueden, S. Saalfeld, B. Schmid, J.-Y. Tinevez, D.J. White, V. Hartenstein, K. Eliceiri, P. Tomancak, A. Cardona, Fiji: an open-source platform for biological-image analysis, Nature Methods 9 (7) (2012) 676–682, http://dx.doi.org/10.1038/nmeth.2019, URL: https://www.nature.com/articles/nmeth.2019.

[20] L. Pedrolli, S. Nadimi, S. Maramizonouz, B.A. Menor, A. López, Kinetic adhesion test to determine particle surface energy, HardwareX 14 (2023) e00437, http://dx.doi.org/10.1016/j.ohx.2023.e00437.

[21] L. Pedrolli, Kinetic Adhesion Test apparatus to determine powder's adhesive surface energy, 2022, http://dx.doi.org/10.5281/ZENODO.7448231.

[22] K.E. Easterling, A.R. Thölén, Surface energy and adhesion at metal contacts, Acta Metall. 20 (8) (1972) 1001–1008, http://dx.doi.org/10.1016/0001-6160(72)90134-4, URL: https://www.sciencedirect.com/science/article/pii/0001616072901344.

[23] W. Nan, M. Pasha, T. Bonakdar, A. Lopez, U. Zafar, S. Nadimi, M. Ghadiri, Jamming during particle spreading in additive manufacturing, Powder Technol. 338 (2018) 253–262, http://dx.doi.org/10.1016/j.powtec.2018.07.030.

[24] J. Raedler, E. Sackmann, On the measurement of weak repulsive and frictional colloidal forces by reflection interference contrast microscopy, Langmuir 8 (3) (1992) 848–853, http://dx.doi.org/10.1021/la00039a019.

[25] J. Waschke, T. Pompe, D. Rettke, S. Schmidt, M. Hlawitschka, Radial profile detection of multiple spherical particles in contact with interacting surfaces, PLOS ONE 14 (2019) e0214815, http://dx.doi.org/10.1371/journal.pone.0214815.

[26] S.C. Chowdhury, J.W. Gillespie, Strain-rate dependent mode I cohesive traction laws for glass fiber-epoxy interphase using molecular dynamics simulations, Composites B 237 (2022) 109877, http://dx.doi.org/10.1016/j.compositesb.2022.109877, URL: https://www.sciencedirect.com/science/article/pii/S1359836822002578.

[27] C.V. Raman., On some applications of Hertz's theory of impact, Phys. Rev. 15 (4) (1920) 277–284, http://dx.doi.org/10.1103/physrev.15.277.

[28] H. Hertz, Ueber die Berührung fester elastischer Körper, J. Reine Angew. Math. 92 (1882) 156–171, URL: https://eudml.org/doc/148490.

[29] R.D. Mindlin, Compliance of elastic bodies in contact, J. Appl. Mech. 16 (3) (1949) 259–268, http://dx.doi.org/10.1115/1.4009973.

[30] R.D. Mindlin, H. Deresiewicz, Elastic spheres in contact under varying oblique forces, J. Appl. Mech. 20 (3) (1953) 327–344, http://dx.doi.org/10.1115/1.4010702.

[31] Y. Tsuji, T. Tanaka, T. Ishida, Lagrangian numerical simulation of plug flow of cohesionless particles in a horizontal pipe, Powder Technol. 71 (3) (1992) 239–250, http://dx.doi.org/10.1016/0032-5910(92)88030-l.

[32] M. Pasha, S. Dogbe, C. Hare, A. Hassanpour, M. Ghadiri, A linear model of elasto-plastic and adhesive contact deformation, Granul. Matter 16 (1) (2014) 151–162, http://dx.doi.org/10.1007/s10035-013-0476-y.